ASME Journal of Engineering for Gas Turbines and Power
Online journal at:
https://asmedigitalcollection.asme.org/gasturbinespower

Experimental Investigation of Particulate Emissions From an Ammonia-Fueled Internal Combustion Engine

Tejashri Patil
Department of Mechanical Engineering,
University of Minnesota,
Minneapolis, MN 55455

Shawn Reggeti
Department of Mechanical Engineering,
University of Minnesota,
Minneapolis, MN 55455

Seamus P. Kane
Department of Mechanical Engineering,
University of Minnesota,
Minneapolis, MN 55455

William F. Northrop
Department of Mechanical Engineering,
University of Minnesota,
Minneapolis, MN 55455

Ammonia combustion is a topic of active research due to the need for fuel decarbonization. Although ammonia does not contain carbon, its use in internal combustion engines (ICEs) may still form nitrogen-containing ultrafine particulate matter. This work investigates particulate emissions from NH_3–H_2–air combustion in a single-cylinder Waukesha cooperative fuel research (CFR) octane engine under a range of hydrogen blending and engine load. Particle size distributions were quantified using a Scanning Mobility Particle Sizer (SMPS). A dual-stage dilution sampling system was used to reduce unburned ammonia concentration and maintain particle concentration within the instrument limits. The engine was motored to measure crankcase particle emissions from lubricant oil atomization. Additionally, 100% hydrogen-fueled experiments were conducted to evaluate the effect of combustion on particulate emissions from lubricant oil atomization without NH_3-based particulate formation. Various ammonia–hydrogen fuel blends were tested to quantify the contribution of ammonia-based particulate matter in the exhaust. The elevated particle number concentration as the ammonia fraction rises suggests that combustion with ammonia leads to higher particulate emissions compared to hydrogen combustion at the equivalent peak in-cylinder pressure. Additionally, the presence of both unburned ammonia and NO_2 in the exhaust indicate that the measured particles may consist of ammonium nitrate based on known chemical mechanisms. Modeling suggests that NH_3 and NO_2 found in cold regions of the combustion chamber have the potential to form gas-phase ammonium nitrate that later condenses to form particles in the exhaust system. [DOI: 10.1115/1.4068030]

Keywords: ultrafine particles, ammonia, ammonium nitrate, SACI

1 Introduction

Interest in ammonia combustion has increased in recent years because it is a carbon-free fuel with higher volumetric energy density than liquid hydrogen [1]. Its use in internal combustion engines (ICEs) has the potential to decarbonize sectors like marine shipping, rail transport, agriculture, and stationary power generation [2]. However, elevated auto-ignition temperature of 923 K, narrow flammability range of 15–28% by volume in air, and low laminar flame speed of ≈7 cm/s challenge the stable operation of ICEs fueled with pure ammonia [3]. Despite its low reactivity, ammonia can be used in ICEs through strategies including increasing compression ratio [4,5] and blending with high flame speed fuels like hydrogen [4,6], gasoline [7], or natural gas [8] to promote ignition and stability. Hydrogen is considered an ideal blending candidate since it is carbon-free [6], has high reactivity, and can be produced on board by ammonia decomposition [9]. Ignition of the fuel–air mixture can be achieved by spark ignition (SI) or by using a high-cetane pilot fuel (e.g., diesel) in a dual fuel compression ignition combustion mode [4,10].

Despite the carbon-free characteristic of ammonia, it is known that ammonia-fueled ICEs emit unburned NH_3, NO_x, and N_2O emissions [11]. In addition, for the first time in the literature, this paper investigates the formation of ultrafine particulate emissions from ammonia-fueled ICEs. Ultrafine particulates are known to cause pulmonary inflammation and adverse cardiovascular changes [12]. Beyond lubricating oil-derived particles, ammonium nitrate (NH_4NO_3) particles may be formed in ammonia-fueled ICEs when unburned ammonia reacts with nitrogen dioxide (NO_2). The stoichiometry of this reaction at temperatures below 175 °C is given by the following equation [13]:

$$2NO_2 + 2NH_3 \rightarrow N_2 + H_2O + NH_4NO_3 \quad (1)$$

The semivolatile nature of ammonium nitrate causes it to evaporate at temperatures above 175 °C and remain in equilibrium with vapor-phase compounds NH_3 and HNO_3 (Eq. (2)). Hence, understanding the formation and gas-to-aerosol phase transition of NH_4NO_3 aerosols in engine exhaust is important

The ICE Forward Conference, The Westin Riverwalk. ICEF2024.
Manuscript received November 28, 2024; final manuscript received January 17, 2025; published online March 21, 2025. Editor: Jerzy T. Sawicki.

$$NH_4NO_3 \leftrightharpoons NH_3 + HNO_3 \quad (2)$$

Incomplete combustion of ammonia, low-temperature regions in the combustion chamber, and misfires cause unburned ammonia emissions [11,14]. Several studies show that blending ammonia with 10–20 vol % hydrogen promotes stable combustion characteristics in SI engines and avoids misfires [4,6,14]. Koike et al. have shown that increasing the hydrogen fuel fraction reduces unburned ammonia emissions but increases NO_x [15]. This finding aligns with their numerical results indicating that adiabatic flame temperature rises proportionally with hydrogen fraction in the mixture.

Lhuillier et al. investigated spark ignition engine performance at a compression ratio of 10.5:1 using NH_3/H_2 blends ranging from 0% to 60% H_2 by volume, and equivalence ratios (ϕ) from 0.6 to 1.2 [6]. They found that NH_3 emissions exceeded 15,000 ppmv under rich conditions. This was attributed to excess fuel and incomplete combustion. Mixtures with higher H_2 fractions exhibited elevated NO_x emissions due to increased flame temperatures, promoting thermal NO_x formation ($T > 1800$ K). NO_x levels reached up to 9000 ppm under lean conditions ($\phi < 1$), while they were <500 ppm, under rich conditions ($\phi > 1$). This behavior is likely because of the thermal deNO_x reaction. Thermal deNO_x occurs when NO_x is reduced in the presence of oxygen at temperatures 1100 K to 1400 K [3]. Westlye et al. studied NO_x emissions from an SI engine operated with a fuel consisting of 80 vol % NH_3 and 20 vol % H_2. The engine speed was maintained at 1000 rpm [14]. The NO emissions peaked around an excess air ratio (λ) of 1.3. They concluded that NO formation stems from N_2 dissociation and fuel-bound nitrogen. NO_2 was around 4% of NO_x ($NO + NO_2$) emissions.

Given that unburned ammonia and NO_x emissions are generally high from ammonia-fueled ICEs, exhaust aftertreatment will likely be necessary. Koike and Suzuoki used a bench top reactor to demonstrate that Cu-ZSM-5 catalyzed adsorber in line with a typical three-way catalyst can mitigate NH_3 emissions from the exhaust [16]. Experiments were conducted in a reactor furnace using supply gases comprising an exhaust mixture under stoichiometric combustion containing 1500 ppm NH_3, 250 ppm NO, 1000 ppm O_2, 10% H_2O, and the remainder N_2. Emissions of NO_2 and N_2O were observed apart from NH_3 and NO at the outlet of the system with the Cu-ZSM-5 adsorber. NO_x was fully mitigated at temperatures exceeding 500 K, and 99% conversion of NH_3 was achieved at ≈570 K. Hence, cold start conditions were believed to contribute to ammonia slip. Koike et al. further performed a cold start study on a four-cylinder SI engine with an onboard ammonia reformer for H_2 blending [9]. In this system, a three-way catalyst was placed upstream of an NH_3 adsorber. Cold start emissions were measured for 6 min. They demonstrated the adsorption of all ammonia flowing into Cu zeolite adsorber after 60 s. However, emissions under lean conditions showed that three-way catalyst produced NO_2. This reaction was believed to have produced ammonium nitrate (NH_4NO_3) based on an analysis of the nitrogen balance.

Beyond its hypothesized formation in ammonia-fueled ICEs, ammonium nitrate formation has been extensively studied in diesel aftertreatment systems and has been validated to occur at temperatures below 275 °C [17]. Ammonia is a key molecule for the selective catalytic reduction (SCR) of NO_x emissions in diesel engine exhaust. The SCR process is based on the reaction between nitrogen oxides (about 95% NO, 5% NO_2, and others) present in the exhaust gases and NH_3 (vaporized from injected urea) in the presence of O_2. The SCR reaction forms ammonium nitrate at low temperatures. Ammonium nitrate can deposit on the catalyst causing temporary deactivation by blocking porous catalyst substrates. Since the ammonia combustion produces unburned NH_3 and NO_x emissions, the possibility of particle emissions in the form of NH_4NO_3 must be considered.

This study investigates particle emissions by a preliminary experimental investigation coupled with a modeling study of ammonium nitrate formation potential. Ammonium nitrate formation through catalytic reaction in diesel SCR [17] and noncatalytic reaction through thermal oxidation of ammonia and nitrogen dioxide have been studied in the literature [18]. It is known that ammonium nitrate aerosols contribute to secondary inorganic aerosols in the atmosphere and are precursors to $PM_{2.5}$ emissions [19,20]. However, its formation through the combustion of ammonia in ICEs where NH_3, NO, and NO_2 are present simultaneously remains insufficiently understood. Investigating the size distribution of particulate emissions from the combustion of ammonia under different engine loads and hydrogen–ammonia fuel blends is an important first step in understanding whether nitrogen-derived particles are formed.

2 Materials and Methods

2.1 Engine and Instrumentation. A Waukesha cooperative fuel research (CFR) octane rating engine was the test platform for this study. The compression ratio was set to 10:1 to explore a wide range of hydrogen–ammonia blends while avoiding knocking at high hydrogen fractions. The spark plug was in the pickup port of the CFR engine, and a Kistler Type 6056A pressure transducer was flush mounted in the side port.

Figure 1 shows a schematic of the experiment layout. Air is supplied by a compressor, dried and decarbonized by a pressure swing absorption system, and metered to the engine using a mass flow controller (Brooks 5853E). The 113 L intake plenum is used to dampen the pressure pulsations of the single-cylinder engine. The intake temperature was regulated to 60 °C for all test conditions using an Omega AHPF-101 process heater. Gaseous fuel was fumigated into the intake air ∼30 cm upstream of the intake valve; flow rates of hydrogen and ammonia were controlled by separate mass flow controllers (Alicat MC-20SLPM and Brooks 5851, respectively). For safe handling of ammonia, a containment system was set up inside the test cell. This consists of the ammonia storage cylinder inside a continuously ventilated cabinet equipped with a compressed air supply for purging ammonia from fuel lines. An ammonia sensor located in the test cell automatically shuts the ammonia off and purges the fuel lines with compressed air if ammonia concentrations in the test cell exceed the Occupational Safety and Health Administration permissive exposure limit of 50 ppm. The engine is equipped with an emergency stop that immediately shuts off the dynamometer and fuel supply.

After combustion in the CFR engine, exhaust products are passed through ∼650 mm of 38 mm diameter tubing before entering the 10 L exhaust plenum. The exhaust tubing and plenum were insulated to prevent heat loss and condensation of exhaust species. The sampling probe for particulate emissions measurement was located just downstream of the exhaust plenum to reduce the impact of pressure pulsations on the instruments. Details of the particulate sampling system and measurement instruments are provided in Sec. 2.2.

High-speed engine control (i.e., spark timing) and low-speed control/data acquisition (e.g., fuel flow rates and temperature measurements) were managed with a cRIO 9074 (“engine controller”) coupled to LabVIEW. High-speed in-cylinder pressure data acquisition was accomplished with a PXI-1042 (“combustion analyzer”) coupled to LabVIEW.

Operating conditions are summarized in Table 1 with corresponding measurement uncertainties where available. The engine was operated at 900 rpm and 10:1 compression ratio under several different fueling scenarios. Baseline particulate levels from lubricating oil were measured for a 100% hydrogen case (combustion baseline) and a motoring case (nonreacting baseline). The impact of ammonia fuel on particulate formation was investigated by gradually increasing the ammonia fuel energy fraction to 25%, 50%, and 75%. A pure ammonia fueling condition (100% NH_3) resulted in frequent misfiring and unstable operation due to low flame speed; thus, 75% NH_3 is the highest ammonia fuel fraction reported in this work. The fuel flow rates of the ammonia–hydrogen blends were adjusted to achieve stoichiometric

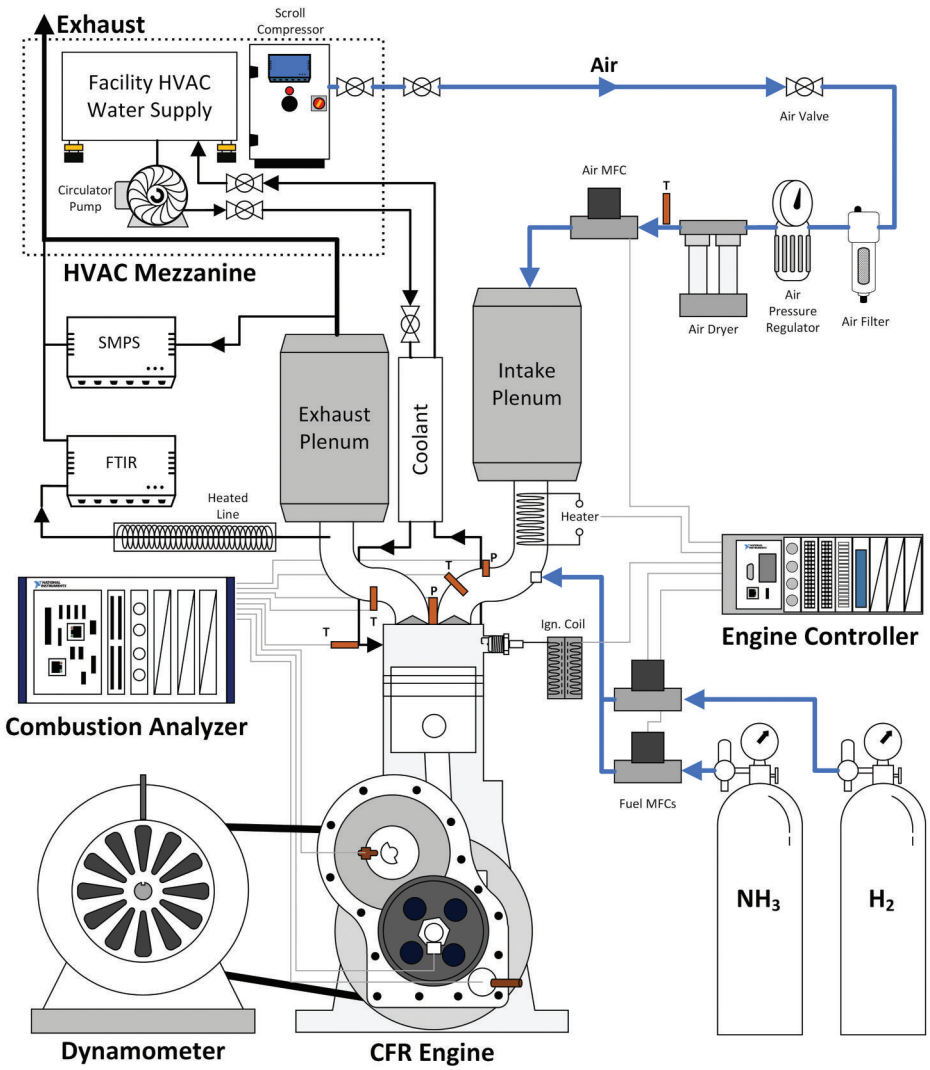

Fig. 1 Layout of components for CFR engine experiments

Table 1 Engine operating conditions

Fuel	Air flow rate (slpm)	H_2 flow rate (slpm)	NH_3 flow rate (slpm)	ϕ_{target}	gIMEP (bar)	Spark timing (deg bTDC)
100% H_2	179.6±15	19.5±0.117	0.015±1	0.26	3.1	18
25% NH_3 + 75% H_2	70.5±15	19.6±0.118	6.6±1	1	3.95	9
50% NH_3 + 50% H_2	72.5±15	12.3±0.074	12.3±1	1	4.1	18
75% NH_3 + 25% H_2	72.6±15	5.6±0.034	16.9±1	1	4.1	32
Motoring	74.5±15	—	—	—	—	—

mixtures and gross indicated mean effective pressure (gIMEP) of 4±0.1 bar. The 100% H_2 fueling case was operated lean to avoid knock, and the gIMEP was limited to 3.1 bar by the H_2 mass flow controller which could supply a maximum flow rate of 20 slpm. For each fueling case, spark timing was set to optimize combustion phasing for maximum gIMEP (maximum brake torque timing).

2.2 Particulate Emissions Measurement. Figure 2 shows the exhaust sampling system and instruments used for particulate measurements. Engine exhaust sample was drawn using a probe with 45 deg cut for particles to follow the exhaust streamline. The exhaust sample was then passed through a two-stage dilution system. Dilution was achieved using ejector pump (EP) diluters with critical orifices upstream of the sample flow. The critical orifices upstream of the ejector pumps were used to maintain a constant volumetric flow rate (choked flow) of the sample flow. An AirVac TD260H ejector pump was used for the first stage operated with dilution air supplied at 4.13 bar. An AirVac TD110H was used for the second stage operated with dilution air supplied at 5.5 bar. The orifice plate diameter of size 1.12 mm was used for the first stage and 0.46 mm for the second stage yielding an overall dilution ratio of 1600:1. The dilution ratio was measured using carbon dioxide as a trace gas and nitrogen as a dilution gas. The dilution ratio was calculated by the ratio of the undiluted to diluted CO_2 concentrations. The concentration of CO_2 postdilution was measured using the iRD analyzer of an AVL emissions bench.

A TSI Scanning Mobility Particle Sizer (SMPS) consisting of Model 3080 Electrostatic Classifier with long-differential mobility analyzer and Model 3025A ultrafine condensation particle counter was used to measure the particle size distribution. SMPS

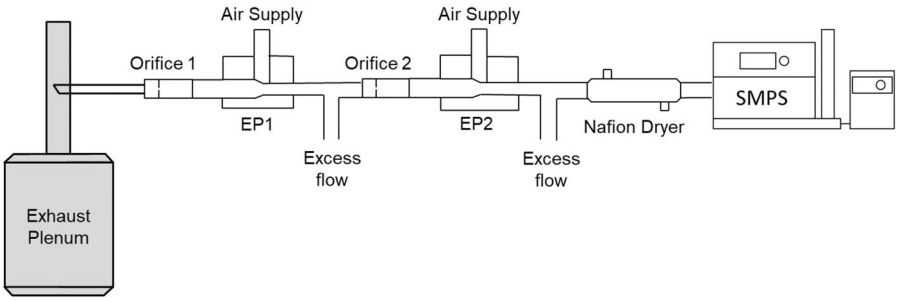

Fig. 2 Particle sampling system showing dilution system and instruments used

measurements were taken at steady-state conditions with a scan time of 120 s. The presented results are an average of three samples measured for each condition. The differential mobility analyzer was operated at high flow mode with 1.5 lpm of aerosol flow rate and 15 lpm sheath air flow rate. The SMPS was calibrated using 1 g/L NaCl solution in de-ionized water prior to engine experiments.

To avoid particle loss due to condensation, the sample entering the dilution stream was maintained at temperatures above the dew point of 80 °C. The sample was passed through a Nafion dryer Perma Pure gas polytube dryer PD-100T-24MSA to ensure the removal of water vapor before entering the SMPS.

2.3 Zero-Dimensional Simulation of Exhaust Species. A zero-dimensional constant temperature–pressure reactor modeling study was performed to further investigate the potential formation of ammonium nitrate in an ammonia-fueled engine. This analysis was performed using CANTERA (version 3.0.0) with MATLAB programing. An ideal gas reactor at engine-like conditions of pressure and temperature was set up using the Stagni 2020 mechanism [21]. The model was run at temperatures ranging from 1200 K to 2600 K at a pressure of 20 bar and residence time of 1 ms, approximating ≈5 deg crank angle of combustion in the engine. The equivalence ratio was kept at stoichiometric, and the hydrogen fuel fraction of the NH_3–H_2 blend was varied from 0% to 100% to investigate the fuel effects on emissions. Although ammonium nitrate is not included in the Stagni mechanism, its primary precursors (NH_3 and NO_2) are interpreted as a proxy for ammonium nitrate formation.

3 Results and Discussion

In-cylinder pressure measurements and apparent heat release rate (AHRR) are shown in Fig. 3. The pure hydrogen fueled case (100% H_2) is the least like the other cases because: (1) it produced less gIMEP than the other cases since the experiment was limited by the H_2 fueling rate, (2) it was operated lean to prevent knocking, and (3) it was operated with boosted intake pressures in attempt to maximize gIMEP. As a result, the cylinder pressures are ≈2–5 bar greater during compression and combustion for the 100% H_2 case compared to the other fuel mixtures. AHRR for the 100% H_2 case is gradual, indicating a flame propagation mode, with a lower peak AHRR in comparison to the other cases since there is fuel energy available.

The remaining cases (75%, 50%, and 25% H_2) all exhibit similar peak cylinder pressures but distinct combustion phenomena, as shown in Fig. 3. The 25% NH_3 + 75% H_2 case operated optimally with a late spark timing (9 deg bTDC, Table 1). After ignition, cylinder pressure rises quickly, resulting in a slightly higher peak pressure, phased later in the cycle compared to the other fuel blends. The AHRR for the 25% NH_3 + 75% H_2 case shows that heat is released quickly around −5 deg aTDC, then AHRR plateaus and quickly increases again around top dead center (TDC) and 15 deg aTDC. These sudden increases in AHRR suggest that a flame partially propagates across the combustion chamber and is then accelerated by an auto-ignition event. Such a phenomenon is not evident with the remaining cases (50% and 25% H_2), which exhibit a more gradual increase in pressure and AHRR after spark timing,

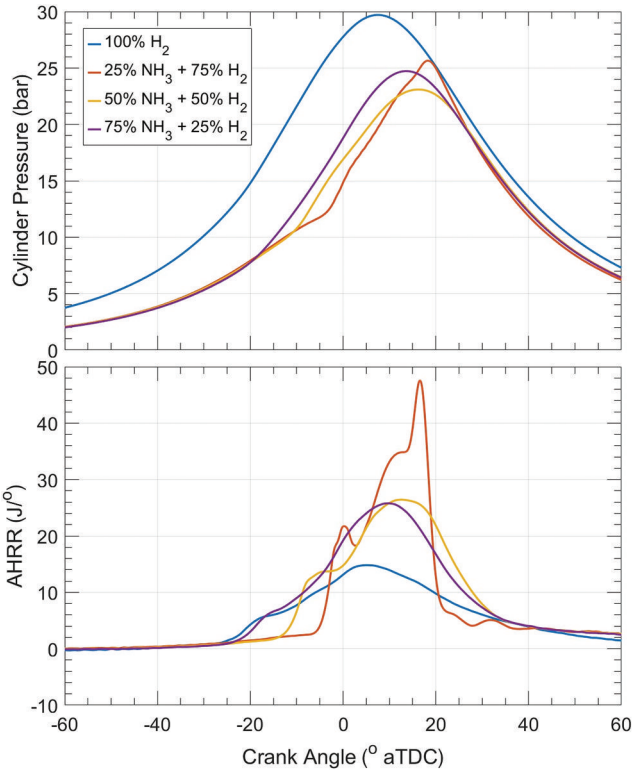

Fig. 3 Engine performance plots: (*a*) cylinder pressure and (*b*) AHRR

suggesting that heat is released as a flame propagates across the combustion chamber.

Particle distributions measured by the SMPS are shown in Fig. 4, and key particle emissions quantities, geometric mean diameter (GMD), and total concentration are shown in Table 2. Figure 4 shows the distribution of particle diameter on the horizontal axis and the total concentration on the vertical axis, illustrating the dispersions of particle emissions of a given size. The nucleation mode is observed which typically consists of particles in the 5–50 nm diameter range [22]. Exhaust dilution and cooling cause volatile compounds to form which are measured during this mode. The particle emissions during engine motoring were measured to be of low total particle concentration compared to the reacting cases. Additionally, motoring particles had a GMD of 33 nm, larger than all of the reacting cases. The total particle concentration for the 100% H_2 case was like the baseline motoring condition but the GMD was significantly smaller, 11.2 nm. Since hydrogen combustion in air is believed to not form any particulate matter, these emissions are hypothesized to be ash, and/or metal additives from the atomization and combustion of lube oil in the hydrogen flame. These results suggest that the motoring condition produces oil aerosol in the engine by piston motion and that these droplets partially burn in the

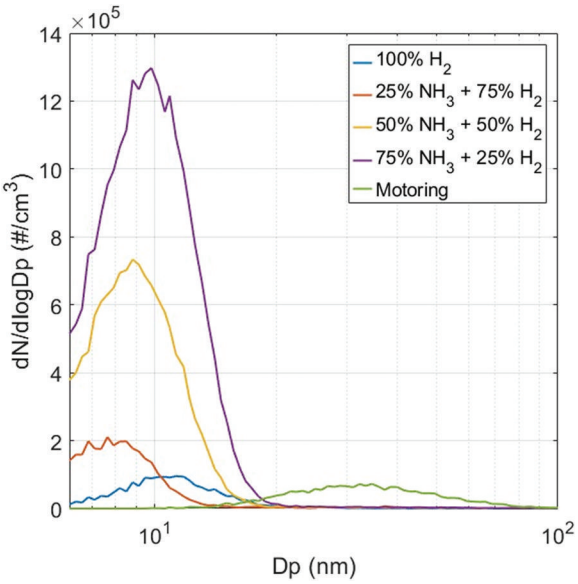

Fig. 4 Particle size distributions measured by SMPS for different fuel blends and engine motoring conditions

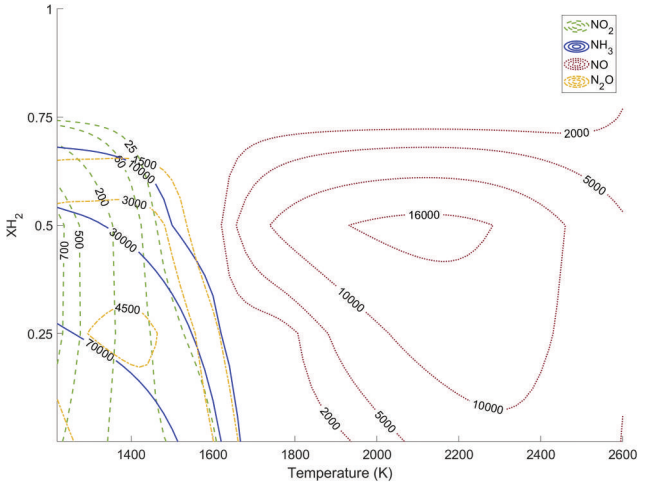

Fig. 5 NH_3–NO_x–N_2O emissions in ppm for combustion with varying fuel blends (at $XH_2 = 0.25$ and $XNH_3 = 0.75$) and temperatures at 20 bar and 1 ms

reacting experiments, reducing their GMD. As such, the 100% H_2 case quantifies the particle emissions that are contributed by the lube oil, and additional particulates detected in the other cases are an effect of the ammonia in the fuel.

Figure 4 shows a clear trend that increasing the ammonia fraction of the fuel increases the total particle concentration in the exhaust. Interestingly, all the NH_3–H_2 fuel blends show a very similar GMD, 9–10 nm. The increasing particle concentration may be due to the formation of ammonium nitrate, which is supported by previous literature investigating ammonia-fueled engines [9] and diesel SCR systems [17]. However, other thermochemical phenomena may also be responsible for the increased particulate emissions which cannot be ruled out. For instance, the lower temperature and increased quenching distance of ammonia flames may change the oil aerosol dynamics. Future experiments are needed to characterize particle composition/morphology and to understand the mechanisms involved in their formation.

The increasing particle concentration with an increase of ammonia fraction suggests that particulate formation is driven by the addition of ammonia in the combustion chamber. The fuel effect on the formation of ammonium nitrate precursors was investigated through zero-dimensional simulation of the combustion process in an ammonia reactor simulating engine-like conditions. The results of the simulation are summarized in Fig. 5 which shows the emissions of NH_3–NO_x–N_2O species for different fuel blends and temperatures. The 25% XH_2 on the vertical axis of Fig. 5 represents 25% H_2 + 75% NH_3 fuel blend, 50% XH_2 represents 50% H_2 + 50% NH_3 blend, and so on. The unburned ammonia emissions were observed at low temperatures. There exists a low-temperature region between 1200 K and 1600 K and the ammonia fraction of 25% to 100% where ammonia and NO_2 are simultaneously present. Such low-temperature regions are known to occur near the walls and in the crevice volumes of the combustion chamber in ICEs.

Table 2 Geometric mean diameter and total particle concentration

Test condition	GMD (nm)	Total concentration (#/cm^3)	Geometric standard deviation
100% H_2	11.2	26,894	1.58
25% NH_3 + 75% H_2	8.8	46,675	1.47
50% NH_3 + 50% H_2	9.1	193,901	1.31
75% NH_3 + 25% H_2	9.7	367,043	1.3
Motoring	32.8	30,724	1.51

In the exhaust, ammonium nitrate formation has been known to form at temperatures below 200 °C through selective catalytic reduction reaction where ammonia is a reducing agent of NO_x emissions [23,24]. Ciardelli et al. presented the reaction scheme (Eqs. (3)–(7)) which yields ammonium nitrate that depends on temperature and feed gas NO_2 fraction [25,26]. Without NO, the first step in the fast SCR reaction is NO_2 dimerization. The dinitrogen tetroxide then disproportionated to form nitric acid (HNO_3) and nitrous acid (HONO). These species then react with ammonia resulting in ammonium nitrite (NH_4NO_2) and ammonium nitrate (NH_4NO_3) formation. Ammonium nitrite readily decomposes into nitrogen and water

$$2NO_2 \longleftrightarrow N_2O_4 \tag{3}$$

$$N_2O_4 + H_2O \rightarrow HONO + HNO_3 \tag{4}$$

$$HONO + NH_3 \rightarrow NH_4NO_2 \tag{5}$$

$$HNO_3 + NH_3 \rightarrow NH_4NO_3 \tag{6}$$

$$NH_4NO_2 \rightarrow N_2 + H_2O \tag{7}$$

Once ammonium nitrate is formed, it reacts with NO by the following reaction:

$$NH_4NO_3 + NO \rightarrow N_2 + NO_2 + 2H_2O \tag{8}$$

The NO_2 formed by reaction (8) can then react further with NH_3 according to reaction (1), thus producing more nitrogen and ammonium nitrate.

Ammonium nitrate was concluded to be an intermediate species of the fast SCR reaction given by Eq. (8) where equimolar NO: NO_2 reacts with ammonia to yield nitrogen and water

$$2NH_3 + NO + NO_2 \rightarrow 2N_2 + 3H_2O \tag{9}$$

At temperatures above 170 °C, ammonium nitrate can undergo reversible endothermic dissociation into ammonia and nitric acid according to equilibrium reaction (2). Between 200 °C and 260 °C, it can exothermically decompose into nitrous oxide (N_2O) and water given by reaction (10)

$$NH_4NO_3 \rightarrow N_2O + 2H_2O \tag{10}$$

In the combustion chamber where NO_2–NH_3 coexist at low temperatures, the formation of ammonium nitrate may occur with NO_2 being the limiting reactant. The presence of N_2O in the same region suggests that ammonium nitrate is dissociated through an exothermic reaction (Eq. (10)). The most likely route to ammonium nitrate formation is in the exhaust where temperatures are below 450 °C. The presence of water vapor in the exhaust potentially influences the ammonium nitrate formation.

The composition of particulate emissions from ammonia combustion in internal combustion engines will be further studied in future work to characterize and confirm the presence of ammonium nitrate. The composition of particle emissions depends on sampling and measurement. In the exhaust stream, ammonium nitrate particles stay in the gas phase. As exhaust is cooled during dilution, it causes particles to condense or adsorb onto existing particles. Heterogeneous nucleation occurs to form larger particles, and volatile materials transform into solid and liquid particulate matter. These are variables that will be investigated thoroughly in future experiments. The formation of ammonium nitrate will also be studied by speciating the exhaust emissions and performing a nitrogen balance study.

4 Conclusion

Particulate formation from an ammonia-fueled single-cylinder Waukesha CFR engine was studied in this work. Beyond oil-derived particulates, this work definitively shows through experimental measurements that ammonia combustion leads to elevated particulate emissions compared to hydrogen only combustion at the same peak cylinder pressure. Further, the simultaneous presence of unburned ammonia and NO_2 in the exhaust suggests that the additional measured particles may consist of ammonium nitrate based on known chemical mechanisms from the literature. Modeling confirms that NH_3 and NO_2 found in cold regions of the combustion chamber have the potential to form gas-phase ammonium nitrate that later condenses to form particles in the exhaust system. In future work, characterization of particle emissions to confirm the hypothesized chemical composition will be performed. A nitrogen balance study will be done to confirm and understand the formation of ammonium nitrate in internal combustion engines.

Funding Data

- U.S. State of Minnesota Session Law, Chapter 4, Article 2, Section 4 for NH_3-fueled power generation research and development.

Data Availability Statement

The authors attest that all data for this study are included in the paper.

Nomenclature

CFR = cooperative fuel research
ICE = internal combustion engine
SCR = selective catalytic reduction
SMPS = Scanning Mobility Particle Sizer

References

[1] MacKenzie, J. J., and Avery, W. H., 1996, "Ammonia Fuel: The Key to Hydrogen-Based Transportation," Proceedings of the 31st Intersociety Energy Conversion Engineering Conference (IECEC 96), Washington, DC, Aug. 11–16, pp. 1761–1766.

[2] Tornatore, C., Marchitto, L., Sabia, P., and De Joannon, M., 2022, "Ammonia as Green Fuel in Internal Combustion Engines: State-of-the-Art and Future Perspectives," Front. Mech. Eng., **8**, p. 944201.

[3] Kobayashi, H., Hayakawa, A., Somarathne, K. D. K. A., and Okafor, E. C., 2019, "Science and Technology of Ammonia Combustion," Proc. Combust. Inst., **37**(1), pp. 109–133.

[4] Reggeti, S., Kane, S., and Northrop, W., 2023, "Experimental Investigation of Spark-Assisted Compression-Ignition With Ammonia-Hydrogen Blends," JAE, **1**(1), pp. 91–105.

[5] Mounaïm-Rousselle, C., Mercier, A., Brequigny, P., Dumand, C., Bouriot, J., and Houillé, S., 2022, "Performance of Ammonia Fuel in a Spark Assisted Compression Ignition Engine," Int. J. Engine Res., **23**(5), pp. 781–792.

[6] Lhuillier, C., Brequigny, P., Contino, F., and Mounaïm-Rousselle, C., 2020, "Experimental Study on Ammonia/Hydrogen/Air Combustion in Spark Ignition Engine Conditions," Fuel, **269**, p. 117448.

[7] Grannell, S. M., Assanis, D. N., Bohac, S. V., and Gillespie, D. E., 2008, "The Fuel Mix Limits and Efficiency of a Stoichiometric, Ammonia, and Gasoline Dual Fueled Spark Ignition Engine," ASME J. Eng. Gas Turbines Power, **130**(4), p. 042802.

[8] Oh, S., Park, C., Oh, J., Kim, S., Kim, Y., Choi, Y., and Kim, C., 2022, "Combustion, Emissions, and Performance of Natural Gas–Ammonia Dual-Fuel Spark-Ignited Engine at Full-Load Condition," Energy, **258**, p. 124837.

[9] Koike, M., Suzuoki, T., Takeuchi, T., Homma, T., Hariu, S., and Takeuchi, Y., 2021, "Cold-Start Performance of an Ammonia-Fueled Spark Ignition Engine With an On-Board Fuel Reformer," Int. J. Hydrogen Energy, **46**(50), pp. 25689–25698.

[10] Hwang, J., Kane, S., and Northrop, W. F., 2018, "Demonstration of Single-Fuel Reactivity Controlled Compression Ignition Using Reformed Exhaust Gas Recirculation," SAE Paper No. 2018-01-0262.

[11] Northrop, W. F., 2024, "Modeling Nitrogen Species From Ammonia Reciprocating Engine Combustion in Temperature-Equivalence Ratio Space," Appl. Energy Combust. Sci., **17**, p. 100245.

[12] Kittelson, D., Khalek, I., McDonald, J., Stevens, J., and Giannelli, R., 2022, "Particle Emissions From Mobile Sources: Discussion of Ultrafine Particle Emissions and Definition," J. Aerosol Sci., **159**, p. 105881.

[13] Mearns, A. M., and Ofosu-Asiedu, K., 1984, "Ammonium Nitrate Formation in Low Concentration Mixtures of Oxides of Nitrogen and Ammonia," J. Chem. Technol. Biotechnol., **34**(6), pp. 350–354.

[14] Westlye, F. R., Ivarsson, A., and Schramm, J., 2013, "Experimental Investigation of Nitrogen Based Emissions From an Ammonia Fueled SI-Engine," Fuel, **111**, pp. 239–247.

[15] Koike, M., Miyagawa, H., Suzuoki, T., and Ogasawara, K., 2012, "Ammonia as a Hydrogen Energy Carrier and Its Application to Internal Combustion Engines," Sustainable Vehicle Technologies, Toyota Central R&D Labs., Inc., Yokomichi, Nagakute, Japan, pp. 61–70.

[16] Koike, M., and Suzuoki, T., 2019, "In-Line Adsorption System for Reducing Cold-Start Ammonia Emissions From Engines Fueled With Ammonia and Hydrogen," Int. J. Hydrogen Energy, **44**(60), pp. 32271–32279.

[17] Ottinger, N., Xi, Y., and Liu, Z. G., 2018, "Formation and Decomposition of Ammonium Nitrate on an Ammonia Oxidation Catalyst," SAE Paper No. 2018-01-0342.

[18] Mearns, A. M., and Ofosu-Asiedu, K., 1984, "Kinetics of Reaction of Low Concentration Mixtures of Oxides of Nitrogen, Ammonia and Water Vapour," J. Chem. Technol. Biotechnol., **34**(6), pp. 341–349.

[19] Wexler, A. S., and Seinfeld, J. H., 1990, "The Distribution of Ammonium Salts Among a Size and Composition Dispersed Aerosol," Atmos. Environ. Part A. Gen. Top., **24**(5), pp. 1231–1246.

[20] Wei, Y., Tian, X., Huang, J., Wang, Z., Huang, B., Liu, J., Gao, J., et al., 2023, "New Insights Into the Formation of Ammonium Nitrate From a Physical and Chemical Level Perspective," Front. Environ. Sci. Eng., **17**(11), p. 137.

[21] Stagni, A., Cavallotti, C., Arunthanayothin, S., Song, Y., Herbinet, O., Battin-Leclerc, F., and Faravelli, T., 2020, "An Experimental, Theoretical and Kinetic-Modeling Study of the Gas-Phase Oxidation of Ammonia," React. Chem. Eng., **5**(4), pp. 696–711.

[22] Kittelson, D. B., 1998, "Engines and Nanoparticles: A Review," J. Aerosol Sci., **29**(5–6), pp. 575–588.

[23] Koebel, M., Madia, G., and Elsener, M., 2002, "Selective Catalytic Reduction of NO and NO_2 at Low Temperatures," Catal. Today, **73**(3–4), pp. 239–247.

[24] Madia, G., Koebel, M., Elsener, M., and Wokaun, A., 2002, "Side Reactions in the Selective Catalytic Reduction of NO_x With Various NO_2 Fractions," Ind. Eng. Chem. Res., **41**(16), pp. 4008–4015.

[25] Ciardelli, C., Nova, I., Tronconi, E., Chatterjee, D., Bandl-Konrad, B., Weibel, M., and Krutzsch, B., 2007, "Reactivity of NO/NO_2–NH_3 SCR System for Diesel Exhaust Aftertreatment: Identification of the Reaction Network as a Function of Temperature and NO_2 Feed Content," Appl. Catal. B: Environ., **70**(1–4), pp. 80–90.

[26] Ciardelli, C., Nova, I., Tronconi, E., Chatterjee, D., and Bandl-Konrad, B., 2004, "A 'Nitrate Route' for the Low Temperature 'Fast SCR' Reaction Over a V_2O_5–WO_3/TiO_2 Commercial Catalyst," Chem. Commun., (23), pp. 2718–2719.